ACADEMIC PRESS

Available online at www.sciencedirect.com

SCIENCE DIRECT®

Journal of Solid State Chemistry 175 (2003) 328–340

JOURNAL OF SOLID STATE CHEMISTRY

http://elsevier.com/locate/jssc

Synthesis, crystal structures and investigations on the dehydration reaction of the new coordination polymers poly[diaqua-(μ_2-squarato-*O*,*O*′)-(μ_2-4,4′-bipyridine-*N*,*N*′)*Me*(II)] hydrate (*Me* = Co, Ni, Fe)

Jan Greve, Inke Jeß, and Christian Näther*

Institut für Anorganische Chemie, Universität zu Kiel, Olshausenstr. 40 (Otto-Hahn-Platz 6-7), D-24098-Kiel, Germany

Received 5 February 2003; received in revised form 8 May 2003; accepted 20 May 2003

Abstract

The three new isostructural coordination polymers poly[diaqua-(μ_2-squarato-*O*,*O*′)-(μ_2-4,4′-bipyridine-*N*,*N*′)*Me*(II)] hydrate (*Me* = Fe, Co, Ni) were prepared by hydrothermal reaction. All compounds are isostructural and crystallize in the monoclinic space group $P2_1/c$ with 4 formula units in the unit cell ($a = 18.893$ (1) Å, $b = 11.450$ (1) Å, $c = 8.0985$ (4) Å, $\beta = 93.032$ (5)°, $V = 1749.5$ (2) Å^3, $[Fe(C_4O_4)(C_{10}H_8)(H_2O)_2] \cdot (H_2O)_3$; $a = 18.937$ (1) Å, $b = 11.342$ (1) Å, $c = 8.0545$ (5) Å, $\beta = 91.83$ (1)°, $V = 1725.3$ (2) Å^3, $[Co(C_4O_4)(C_{10}H_8)(H_2O)_2] \cdot (H_2O)_3$; $a = 18.271$ (1) Å, $b = 11.340$ (1) Å, $c = 7.8946$ (4) Å, $\beta = 90.69$ (5)°, $V = 1633.1$ (2) Å^3, $[Ni(C_4O_4)(C_{10}H_8)(H_2O)_2](H_2O)_{1.7}$). In the crystal structures the metal atoms are coordinated by two squarate dianions, two 4,4′-bipyridine ligands and two water molecules. The metal atoms are connected via the squarate dianions and the 4,4′-bipyridine ligands into layers, which interpenetrate forming a three-dimensional coordination network. This arrangement yields channels in which additional water molecules are embedded. Thermoanalytic investigations show that upon heating the channel water is removed in the first step and that the water coordinated to the metal atoms is emitted in the second step. Both steps are fully reversible with the former reaction proceeding via a topotactic reaction. The hydration and dehydration of the compounds are accompanied with a continuous change of the color of the materials. The de- and reintercalation processes were investigated using single crystal structure analysis, X-ray powder diffraction, temperature-dependent X-ray powder diffraction, simultaneous differential thermoanalysis and thermogravimetry coupled to mass spectroscopy, differential scanning calorimetry and time-dependent UV-Vis spectroscopy. The results of the investigations are discussed and compared with those for the previously reported manganese compound.

Keywords: Coordination polymers; Synthesis; Crystal structure; Thermoanalytic investigations; Optical properties; Dehydration; Topotactic reaction

1. Introduction

Recently, the development of strategies for a more directed construction of multidimensional coordination networks and architectures has attracted much interest [1–13]. It has been shown that based on simple considerations concerning the nature of the metal atoms, the size, shape and coordination behavior of the ligands as well as the stoichiometry of the building blocks the structures of such coordination polymers can be predetermined to some extend [1–13]. Because the structure of the solids is unambiguously connected with their physical properties, such strategies are of extraordinary interest for the preparation of compounds with desired physical properties like cooperative magnetic phenomena, ion exchange, molecular sieving or host-guest inclusion chemistry [14–30]. Therefore, a large number of such compounds were structurally characterized and investigated during the last years.

In our own investigations we have prepared new coordination polymers based on transition metal squarates and aromatic amine ligands like pyrazine [31,32] or 4,4′-bipyridine [33]. In one of these compounds based on manganese and 4,4′-bipyridine two-dimensional interpenetrating coordination networks were found in which the metal atoms are coordinated by two squarate dianions, two 4,4′-bipyridine molecules and two water molecules forming channels along the crystallographic *c*-axis. The channels are filled with additional water

*Corresponding author. Fax: +49-0-431-880-1520.
E-mail address: cnaether@ac.uni-kiel.de (C. Näther).

0022-4596/03/$ - see front matter © 2003 Elsevier Inc. All rights reserved.
doi:10.1016/S0022-4596(03)00306-2

molecules that are not coordinated to the metal atoms. Additional investigations using thermoanalytic and X-ray powder diffraction demonstrate that the channel water molecules as well as the water which are coordinated to the manganese atoms can be reversibly deintercalated and reintercalated. This reaction is accompanied with a change of the color of the material. Starting from these findings we have prepared and structurally characterized the corresponding compounds with Fe, Co and Ni. The properties of these new compounds were investigated using differential thermoanalysis (DTA), thermogravimetry (TG) coupled with mass spectroscopy (MS), differential scanning calorimetry (DSC), X-ray powder diffraction, temperature-dependent X-ray powder diffraction and UV spectroscopy. Here we report the results of our investigations.

2. Experimental section

2.1. Synthesis

The title compounds were prepared by the reaction 0.5 mmol of the metal halogenide ($FeCl_2 \cdot 4H_2O$ (Merck), $CoBr_2$ (Alfa), $NiBr_2$ (Aldrich)), 0.5 mmol squaric acid (ACROS) and 1.0 mmol 4,4′-bipyridine (ACROS) in 10 ml water in Teflon-lined steel autoclaves at 150°C. After 5 days the reaction mixture was cooled down to room temperature and the products were filtered off and washed with water. The products consist of a pure microcrystalline powder of the title compounds with crystals being too small for single crystal X-ray analysis. The excess of 4,4′-bipyridine is necessary for the neutralization of the squaric acid. Otherwise, no pure samples could be obtained. Yield: 74–82% based on the metal halides. The homogeneity of all products was checked by X-ray powder diffraction and elemental analysis. It must be noted that the actual water content depends on how the samples were stored. Elemental analysis: poly[diaqua-(μ_2-squarato-*O*,*O*′)-(μ_2-4,4′-bipyridine-*N*,*N*′)-Fe(II)] trihydrate calc.: C: 40.60%, N: 6.76%, H: 4.38%; found: C: 40.39%, N: 6.69%, H: 4.11%; poly[diaqua-(μ_2-squarato-*O*,*O*′)-(μ_2-4,4′-bipyridine-*N*,*N*′)-Co(II)] trihydrate calc.: C: 40.30%, N: 6.71%, H: 4.35%; found: C: 40.42%, N: 6.83%, H: 4.22%; poly[diaqua-(μ_2-squarato-*O*,*O*′)-(μ_2-4,4′-bipyridine-*N*,*N*′)-Ni(II)] trihydrate calc.: C: 40.33%, N: 6.72%, H: 4.35%; found: C: 40.37%, N: 6.85%, H: 4.18%.

Single crystals were prepared using the reaction conditions described above but with 0.5 mmol of 4,4′-bipyridine. After 7 days the reaction mixture was cooled down with 3°C/h. In this case large single crystals of the title compounds could be isolated which contain small crystals of the metal squarate hydrates as the second phase (Fe [34,35], Co [34,36], Ni [37,38]).

2.2. Single crystal structure analysis

All investigations were performed with an Imaging Plate Diffraction System (IPDS) from STOE & CIE. The structure solutions were performed with direct methods using SHELXS-97 [39] and structure refinements were performed against F^2 using SHELXL-97 [40]. For the Fe and Co compound numerical absorption corrections were applied using X-Red [41] and X-Shape [42]. All non-hydrogen atoms were refined with anisotropic displacement parameters. The C–H hydrogen atoms were positioned with idealized geometry (dC–H = 0.95 Å) and refined with fixed isotropic displacement parameters (U_{eq}(H) = 1.2 · U_{eq}(C)) using the riding model. The O–H hydrogen atoms were located in the difference map and the O–H bond lengths were positioned with idealized bond lengths of 0.82 Å and were refined with fixed isotropic displacement parameters (U_{eq}(H) = 1.5 · U_{eq}(O)) using the riding model. In the crystal investigated for the Ni compound the positions of the channel water molecules are not fully occupied. Therefore, the site occupation factors of each atom were refined yielding 1.7 channel water molecules per formula unit. Details of the structure determination, atomic coordinates and isotropic displacement parameters as well as lists with selected bond lengths, angles and hydrogen bonding parameters are given in Tables 1–6.

Crystallographic data (excluding structure factors) for the structures reported in this paper have been deposited with the Cambridge Crystallographic Data Centre as supplementary publication no. CCDC 213650 (Fe), CCDC 213652 (Co) and CCDC 213651 (Ni). Copies of the data can be obtained, free of charge, on application to CCDC, 12 Union Road, Cambridge CB2 1 EZ, UK. (fax: +44-(0)1223-336033 or E-mail: deposit@ccdc.cam.ac.uk).

2.3. X-ray powder diffraction

Powder diffraction experiments were performed using a STOE STADI P transmission powder diffractometer with Cu$K\alpha$-radiation (λ = 154.0598 pm) and a Siemens D-5000 diffractometer with Cu$K\alpha$-radiation (λ = 154.0598 pm). For temperature- or time-resolved X-ray powder diffraction the diffractometer is equipped with a graphite oven and a position sensitive detector (scan range: 5–50°) from STOE & CIE. All temperature-resolved X-ray powder experiments were performed in glass capillaries under a static air atmosphere.

2.4. Differential thermal analysis, thermogravimetry and mass spectroscopy

DTA-TG measurements were performed simultaneous in Al_2O_3 crucibles using a STA-429 balance from

Table 1
Crystal data and results of the structure refinement for the Fe, Co and Ni compound

Compound	Fe	Co	Ni
MG (g/mol)	414.15	417.23	394.22
Crystal color/shape	orange-red block	light pink block	light blue block
Crystal size (mm)	$0.19 \times 0.12 \times 0.08$	$0.13 \times 0.10 \times 0.06$	$0.08 \times 0.07 \times 0.06$
a (Å)	18.893 (1)	18.937 (1)	18.271 (1)
b (Å)	11.450 (1)	11.342 (1)	11.340 (1)
c (Å)	8.0985 (4)	8.0545 (5)	7.8946 (4)
β (Å^3)	93.032 (5)	91.83 (1)	90.69 (1)
V (Å^3)	1749.5 (2)	1725.3 (2)	1633.1 (2)
Temperature (K)	170	170	170
Crystal system	Monoclinic	Monoclinic	Monoclinic
Space group	$P2_1/c$	$P2_1/c$	$P2_1/c$
Z	4	4	4
$d_{calc.}$ (g cm^3)	1.572	1.606	1.603
μ (mm^{-1})	0.91	1.05	1.23
Min./max. transm.	0.7732/0.9070	0.7817, 0.9446	—
Scan range	$3^\circ \leqslant 2\theta \leqslant 56^\circ$	$3^\circ \leqslant 2\theta \leqslant 56^\circ$	$3^\circ \leqslant 2\theta \leqslant 56^\circ$
Index range	$-24 \leqslant h \leqslant 24$	$24 \leqslant h \leqslant 25$	$24 \leqslant h \leqslant 23$
	$-15 \leqslant k \leqslant 15$	$-14 \leqslant k \leqslant 14$	$-14 \leqslant k \leqslant 14$
	$-10 \leqslant l \leqslant 10$	$-10 \leqslant l \leqslant 10$	$-9 \leqslant l \leqslant 9$
Refl. collected	17029	16630	14577
Independent refl.	4058	4034	3620
Refl. $F_o < 4\sigma(F_o)$	2488	3030	3230
R_{int} (%)	0.0579	0.0532	0.0248
Parameters	239	239	242
R_1 ($F_o < 4\sigma(F_o)$)	0.0459	0.0444	0.0319
WR_2 (all refl.)	0.1260	0.1273	0.0858
GOOF	1.027	1.094	1.106
δF (e Å^{-3})	0.36/−0.57	0.42/−0.50	0.43/−0.49

Table 2
Atomic coordinates ($\times 10^4$) and isotropic displacement parameters (Å$^2 \times 10^3$) for the Fe compound

	x	y	z	U_{eq}
Fe1	5000	10000	5000	14 (1)
O(1)	4553 (1)	9659 (2)	7348 (2)	19 (1)
C(1)	4804 (2)	9843 (2)	8798 (3)	16 (1)
C(2)	5329 (2)	10659 (2)	9579 (3)	16 (1)
O(2)	5711 (1)	11464 (2)	9084 (2)	20 (1)
O(5)	5467 (1)	11560 (2)	5843 (2)	21 (1)
Fe2	10000	5000	10000	14 (1)
O(3)	10369 (1)	5481 (2)	7656 (2)	21 (1)
C(3)	10159 (2)	5208 (3)	6205 (3)	17 (1)
C(4)	10307 (2)	5682 (2)	4576 (3)	16 (1)
O(4)	10674 (1)	6512 (2)	4090 (2)	21 (1)
O(6)	10462 (1)	6541 (2)	10866 (2)	20 (1)
N(1)	5956 (1)	9081 (2)	6030 (3)	19 (1)
C(11)	7155 (2)	7867 (3)	7357 (3)	20 (1)
C(12)	6483 (2)	7350 (3)	7259 (4)	24 (1)
C(13)	5907 (2)	7980 (3)	6605 (4)	23 (1)
C(14)	6601 (2)	9576 (3)	6148 (4)	23 (1)
C(15)	7204 (2)	9010 (3)	6793 (4)	24 (1)
N(2)	8986 (1)	5961 (2)	9270 (3)	20 (1)
C(21)	7785 (2)	7219 (3)	8023 (4)	19 (1)
C(22)	8350 (2)	7779 (3)	8864 (4)	25 (1)
C(23)	8928 (2)	7123 (3)	9468 (4)	26 (1)
C(24)	8437 (2)	5421 (3)	8461 (4)	24 (1)
C(25)	7838 (2)	6007 (3)	7824 (4)	24 (1)
O(7)	6831 (2)	3666 (3)	7452 (3)	38 (1)
O(8)	7526 (2)	2651 (3)	4899 (3)	41 (1)
O(9)	8217 (2)	1319 (3)	7296 (3)	39 (1)

Table 3
Atomic coordinates ($\times 10^4$) and isotropic displacement parameters (Å$^2 \times 10^3$) for the Co compound

	x	y	z	U_{eq}
Co(1)	5000	10000	5000	13 (1)
O(1)	4557 (1)	9641 (2)	7311 (2)	18 (1)
C(1)	4808 (1)	9845 (2)	8775 (3)	15 (1)
C(2)	5337 (1)	10649 (2)	9598 (3)	15 (1)
O(2)	5733 (1)	11448 (2)	9121 (2)	19 (1)
O(5)	5445 (1)	11564 (2)	5865 (2)	20 (1)
Co(2)	10000	5000	10000	13 (1)
O(3)	10358 (1)	5497 (2)	7689 (2)	19 (1)
C(3)	10152 (1)	5214 (2)	6228 (3)	16 (1)
C(4)	10318 (1)	5673 (2)	4592 (3)	16 (1)
O(4)	10699 (1)	6497 (2)	4134 (2)	20 (1)
O(6)	10454 (1)	6534 (2)	10894 (2)	18 (1)
N(1)	5939 (1)	9101 (2)	6054 (3)	17 (1)
C(11)	7147 (1)	7868 (2)	7348 (3)	19 (1)
C(12)	6478 (1)	7353 (2)	7293 (3)	22 (1)
C(13)	5895 (1)	7999 (2)	6656 (3)	21 (1)
C(14)	6584 (1)	9596 (2)	6122 (3)	21 (1)
C(15)	7195 (1)	9022 (2)	6757 (4)	23 (1)
N(2)	9001 (1)	5950 (2)	9224 (3)	19 (1)
C(21)	7788 (1)	7212 (2)	7996 (3)	19 (1)
C(22)	8368 (1)	7783 (2)	8823 (4)	26 (1)
C(23)	8950 (1)	7121 (2)	9412 (4)	25 (1)
C(24)	8442 (1)	5408 (2)	8438 (4)	24 (1)
C(25)	7834 (1)	5997 (3)	7818 (4)	24 (1)
O(7)	6823 (1)	3642 (2)	7515 (3)	38 (1)
O(8)	7529 (1)	2769 (3)	4881 (3)	40 (1)
O(9)	8222 (1)	1320 (2)	7225 (3)	36 (1)

Netzsch. Several measurements under argon and air atmosphere with heating rates of 1 and 4°C/min were performed. DTA-TG-MS measurements were performed simultaneous using the STA-409CD with Skimmer coupling from Netzsch, which is equipped with a quadrupole mass spectrometer QMA 400 (max. 512 amu) from Balzers. The MS measurements were performed in analog and trend scan mode in Al_2O_3 crucibles under a dynamic helium atmosphere (purity: 4.6) using heating rates of 4°C/min. All measurements were performed with a flow rate of 75 ml/min and were corrected for buoyancy and current effects.

2.5. Differential scanning calorimetry

DSC experiments were performed with the DSC 204/1/F from Netzsch. The measurements were performed in bei aluminum crucibles. For all modifications heating and cooling curves were measured using heating rates of 3°C /min. The calorimeter was calibrated using standard reference substances. All characteristic temperatures as well as all enthalpies were estimated from different measurements at 3°C/min.

2.6. CHN analysis

CHN-O-RAPID combustion analyzer from Heraeus. Elemental analysis (%) calculated for the dehydrated samples: $FeC_{14}O_4N_2H_8$: C: 51.89, N: 8.64, H: 2.49; found: C: 51.53, N: 8.42, H: 2.60. $CoC_{14}O_4N_2H_8$: C: 51.40, N: 8.56, H: 2.46; found: C: 51.55, N: 8.48, H: 2.40. $NiC_{14}O_4N_2H_8$: C: 51.44, N: 8.57, H: 2.47; found: C: 51.40, N: 8.61, H: 2.44.

Table 4
Atomic coordinates ($\times 10^4$) and isotropic displacement parameters ($Å^2 \times 10^3$) for the Ni compound

	x	y	z	U_{eq}
Ni(1)	5000	10000	5000	6 (1)
O(1)	4524 (1)	9688 (1)	7282 (2)	10 (1)
C(1)	4793 (1)	9869 (1)	8754 (2)	8 (1)
C(2)	5371 (1)	10612 (1)	9588 (2)	9 (1)
O(2)	5813 (1)	11375 (1)	9108 (2)	14 (1)
O(5)	5443 (1)	11585 (1)	5857 (2)	13 (1)
Ni(2)	10000	5000	10000	9 (1)
O(3)	10017 (1)	4175 (1)	7656 (2)	15 (1)
C(3)	10011 (1)	4638 (2)	6217 (2)	13 (1)
C(4)	10292 (1)	5717 (2)	5462 (3)	18 (1)
O(4)	10648 (1)	6586 (2)	6033 (2)	47 (1)
O(6)	10698 (1)	6344 (1)	9364 (2)	14 (1)
N(1)	5940 (1)	9116 (1)	5970 (2)	10 (1)
C(11)	7181 (1)	7857 (2)	7179 (2)	12 (1)
C(12)	6484 (1)	7363 (2)	7191 (2)	15 (1)
C(13)	5882 (1)	8022 (2)	6602 (2)	14 (1)
C(14)	6611 (1)	9592 (2)	5956 (2)	13 (1)
C(15)	7241 (1)	9003 (2)	6562 (3)	14 (1)
N(2)	9068 (1)	5925 (1)	9085 (2)	12 (1)
C(21)	7838 (1)	7188 (2)	7824 (2)	12 (1)
C(22)	8404 (1)	7743 (2)	8768 (2)	13 (1)
C(23)	9000 (1)	7081 (2)	9396 (2)	14 (1)
C(24)	8527 (1)	5391 (2)	8153 (2)	15 (1)
C(25)	7903 (1)	5980 (2)	7519 (2)	15 (1)
O(7)	6943 (2)	3333 (4)	7633 (6)	38 (2)
O(8)	7471 (2)	3676 (3)	4617 (4)	61 (1)
O(9)	7787 (2)	1683 (4)	6389 (6)	38 (1)

Table 6
Selected bond lengths (Å) and angles (°) for the Mn, Fe, Co and Ni compound

	Mn	Fe (I)	Co (II)	Ni (III)	
*Me*1–O1	2.190 (1)	2.157 (2)	2.136 (2)	2.075 (2)	(×2)
*Me*1–O5	2.160 (2)	2.091 (2)	2.064 (2)	2.069 (2)	(×2)
*Me*1–N1	2.290 (2)	2.215 (3)	2.169 (2)	2.096 (2)	(×2)
*Me*2–O3	2.159 (2)	2.129 (2)	2.103 (2)	2.075 (2)	(×2)
*Me*2–O6	2.146 (2)	2.074 (2)	2.048 (2)	2.067 (2)	(×2)
*Me*2–N2	2.320 (2)	2.261 (3)	2.227 (2)	2.094 (2)	(×2)
O5–*Me*1–O1	87.9 (1)	87.4 (1)	87.4 (1)	87.7 (1)	(×2)
O5–*Me*1–O1	92.1 (1)	92.6 (1)	92.7 (1)	92.3 (1)	(×2)
O1–*Me*1–N1	85.1 (1)	86.1 (1)	86.1 (1)	88.6 (1)	(×2)
O1–*Me*1–N1	94.9 (1)	93.9 (1)	93.9 (1)	91.4 (1)	(×2)
O5–*Me*1–N1	93.0 (1)	92.2 (1)	91.8 (1)	90.1 (1)	(×2)
O5–*Me*1–N1	87.0 (1)	87.8 (1)	88.2 (1)	89.9 (1)	(×2)
O5–*Me*1–O5	180.0	180.0	180.0	180.0	
O1–*Me*1–O1	180.0	180.0	180.0	180.0	
N1–*Me*1–N1	180.0	180.0	180.0	180.0	
O6–*Me*2–O3	87.0 (1)	86.0 (1)	86.0 (1)	85.7 (1)	(×2)
O6–*Me*2–O3	93.1 (1)	94.0 (1)	94.0 (1)	94.3 (1)	(×2)
O3–*Me*2–N2	86.3 (1)	87.4 (1)	86.8 (1)	88.3 (1)	(×2)
O3–*Me*2–N2	93.7 (1)	92.7 (1)	93.3 (1)	91.7 (1)	(×2)
O6–*Me*2–N2	90.9 (1)	90.6 (1)	90.8 (1)	92.7 (1)	(×2)
O6–*Me*2–N2	89.1 (1)	89.4 (1)	89.2 (1)	87.3 (1)	(×2)
O6–*Me*1–O6	180.0	180.0	180.0	180.0	
O3–*Me*1–O3	180.0	180.0	180.0	180.0	
N2–*Me*1–N2	180.0	180.0	180.0	180.0	

Table 5
Selected crystal parameters for the Mn, Fe, Co and Ni compound

Compound	Mn	Fe	Co	Ni
a (Å)	18.716 (1)	18.893 (1)	18.937 (1)	18.271 (1)
b (Å)	11.544 (1)	11.450 (1)	11.342 (1)	11.340 (1)
c (Å)	8.1738 (5)	8.0985 (4)	8.0545 (5)	7.8946 (4)
β (°)	90.54 (1)	93.03 (1)	91.83 (1)	90.69 (1)
V (Å^3)	1766.0 (2)	1749.5 (2)	1725.3 (2)	1633.1 (2)
Water content	5	5	5	3.7
Channel vol. (Å^3)	382	371	357	295

2.7. UV-Vis measurements

UV-Vis spectra were collected using a Varian Cary 5 UV-Vis spectrometer. The measurements were carried out in reflection geometry using a "Ulbricht-Kugel" and $BaSO_4$ as the standard. The reflectance spectra were corrected against the $BaSO_4$ standard and converted into absorption spectra using the Kubelka-Munk function.

2.8. Magnetic measurements

The magnetic measurements were performed using a Physical Property Measuring System (PPMS) from Quantum Design which is equipped with a 9 T magnet. The data were corrected for Core diamagnetism. The fitting of the susceptibility curves was performed in the range between 4 and 300 K for the original sample and that where the channel water molecules were removed and between 30 and 300 K for the completely dehydrated sample which shows an antiferromagnetic ordering. Results of the analysis for the Mn compound: Fully hydrated compound: C = 4.34 (1), μ_B/Mn = 5.89, $\theta = -5.1(1)$ K; Compound in which the channel water was removed: C = 4.32 (1), μ_B/Mn = 5.88, $\theta = -14.0$ (1); Fully dehydrated compound: C = 4.41 (2), μ_B/Mn = 5.94, $\theta = -2.23$ (3).

3. Results and discussion

3.1. Crystal structures

The three new compounds poly[diaqua-(μ_2-squarato-*O*,*O*′)-(μ_2-4,4′-bipyridine-*N*,*N*′)-iron(II)] hydrate, poly [diaqua-(μ_2-squarato-*O*, *O*′)-(μ_2-4, 4′-bipyridine-*N*, *N*′)-cobalt(II)] hydrate and poly[diaqua-(μ_2-squarato-*O*,*O*′)-(μ_2-4,4′-bipyridine-*N*,*N*′)-nickel(II)] hydrate, crystallize in the monoclinic space group $P2_1/c$ with four formula units in the unit cell. All compounds are isotypic to the previously reported Mn compound [33]. In the crystal structure the metal atoms are coordinated by two squarate dianions, two 4,4′-bipyridine ligands and two water molecules within distorted octahedra (Fig. 1). The 4,4′-bipyridine ligand and the two water molecules are located in general positions whereas the metal atoms as well as the two crystallographically independent squarate dianions are located on centers of inversion.

The metal atoms are connected by the squarate dianions via μ-O,O coordination forming "zig-zag" chains in the direction of the crystallographic *c*-axis (Fig. 2). Only one oxygen atom of each squarate dianions is involved in metal coordination and the direct coordination in which two neighbored oxygen atoms are involved is not found. The metal atoms are located nearly in the molecular plane of the squarate dianions and are oriented in the direction of the oxygen lone-pair.

The 4,4′-bipyridine ligands connect the metal atoms into linear chains (Fig. 2). The metal atoms deviate only slightly from the plane of the six-membered bipyridine rings and are oriented in the direction of the N–N vector. From this arrangement layers are formed parallel to (010) which contain large pores (Fig. 2). These layers interpenetrate with symmetry equivalent layers related by the 2_1-screw axis. The connection of the interpenetrating layers is achieved via O–H···O hydrogen bonding between the hydrogen atoms of the water

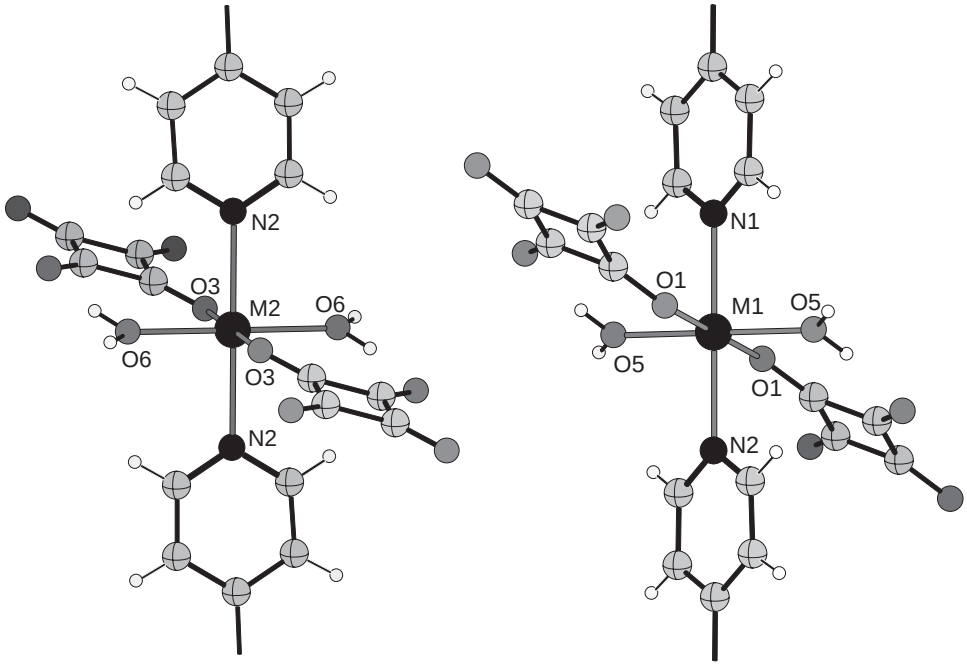

Fig. 1. Crystal structure of the title compounds with view of the metal coordination and labelling (*M* = ●, O = ○, N = ●, C = ◐, H = ○).

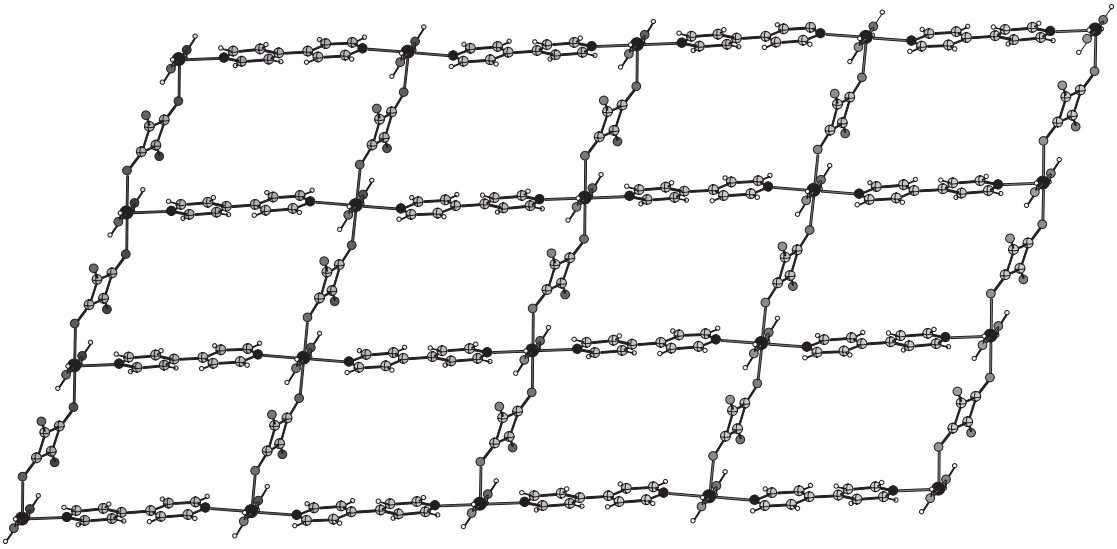

Fig. 2. Crystal structure of the title compounds with view on the two-dimensional coordination network (M = ●, O = ○, N = ●, C = ◍, H = ○).

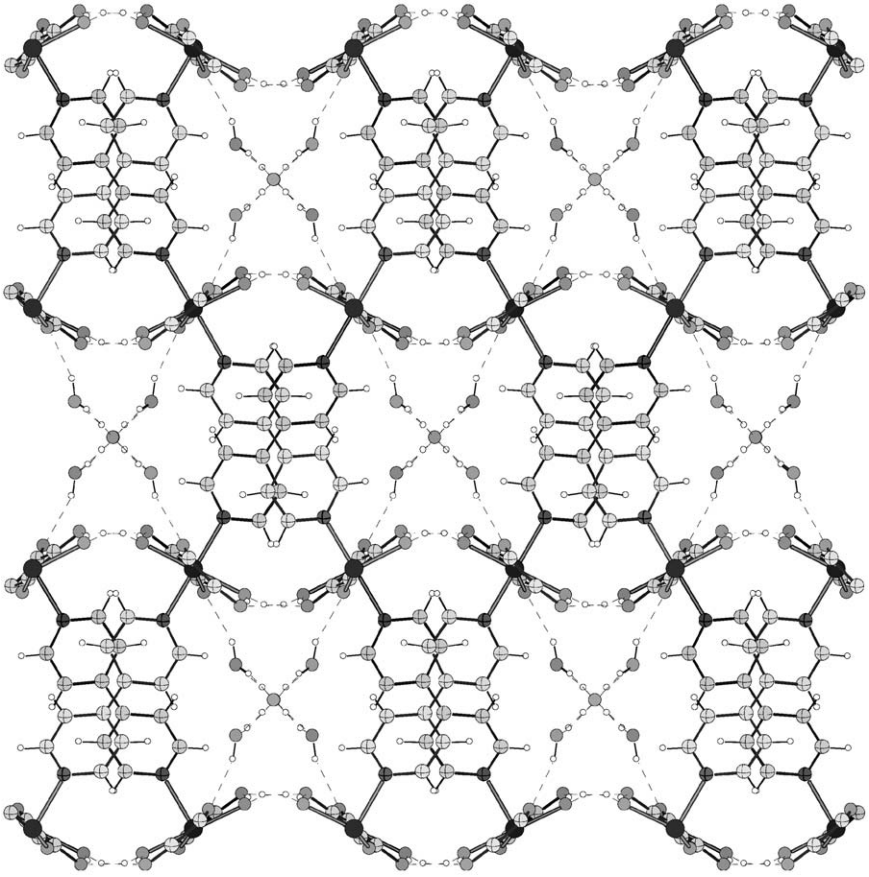

Fig. 3. Crystal structure of the title compounds with view along the crystallographic c-axis (hydrogen bonding is shown as dotted lines; M = ●, O = ○, N = ●, C = ◍, H = ○).

molecules bound to the metal atoms and the squarate oxygen atoms (Fig. 3).

The interpenetrating layers form a three-dimensional coordination network which contains channels in the direction of the crystallographic c-axis (Figs. 3 and 4). In these channels additional water molecules are found that are connected via O–H···O hydrogen bonds to the squarate oxygen atoms and that are named "channel water molecules" in this work.

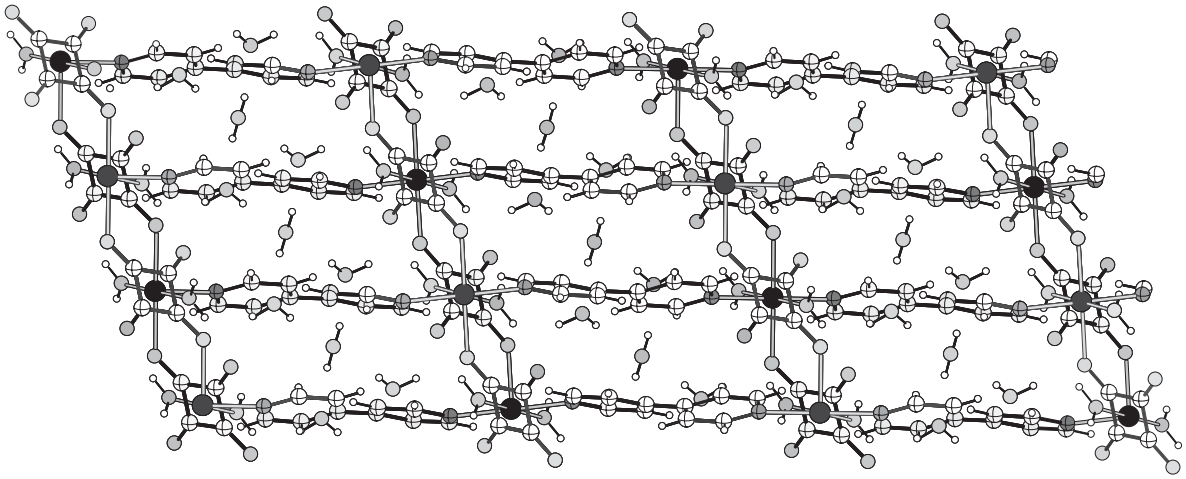

Fig. 4. Crystal structure of the title compounds with view along the crystallographic *b*-axis (*M* = ●, O = ○, N = ◕, C = ◍, H = ○).

Three channel water molecules were found in the Mn, Fe and Co compounds whereas the single crystal investigated for the Ni compound contains only about 1.7 water molecules. We have investigated several crystals of all compounds and we have always found a different channel water content. It must be pointed out that the water content strongly depends on the history of the samples because the channel water molecules can easily be removed (see thermoanalytic investigations).

Because the Ni compound contains a lower water content its structure can only be compared to some extend with the Mn, Fe and Co analogous compounds. But, as expected the unit-cell volume decreases from Mn to Ni with decreasing ionic radii [43,44] and a similar behavior is found for the channel volume which was calculated using Platon (Table 5). Therefore, it might be that for the Ni compound the channels are too small to incorporate three water molecules or this is energetically unfavorable. For the unit cell axes a different behavior is found. Whereas the *b*- and *c*-axis decrease from Mn to Ni the *a*-axis increases except for the Ni compound because of its lower water content (Table 5).

As expected the Me–O and Me–N bond lengths decrease with decreasing ionic radii of the metal atoms and are in the range found for similar structures retrieved from the Cambridge Structure Database [45,46] (Table 6). It must be noted that the Me–O bond lengths to the oxygen atoms of the water molecules are slightly shorter than those to the negatively charged oxygen atoms of the squarate dianions.

As pointed out before, the interpenetrating layers are connected via O–H···O hydrogen bonding between the hydrogen atoms of the water molecules bound to the metal atoms and the squarate oxygen atoms. Intermolecular bond lengths and angles show that this must be a strong interaction (Table 7). Two of the four hydrogen bonds increase from Mn to Ni whereas the others show an opposite trend (Table 7). Therefore, it is difficult to estimate the strength of these interaction as function of the metal atom.

Table 7
Selected bond lengths (Å) and angles (°) for the hydrogen bonding in the Mn, Fe, Co and Ni compound

	Mn	Fe	Co	Ni
O5···O2	2.719	2.643	2.643	2.629
H1···O2	1.922	1.843	1.839	1.834
O5–H1–O2	163.6	164.9	166.3	162.8
O5···O2′	2.664	2.726	2.732	2.797
H2···O2′	1.865	1.918	1.919	1.994
O5–H1–O2′	164.3	171.0	165.8	162.8
O6–O4	2.687	2.695	2.704	2.696
H3–O4	1.901	1.884	1.890	1.879
O6–H3–O4	160.3	169.9	171.6	174.1
O6–O4′	2.638	2.621	2.617	2.641
H4–O4′	1.850	1.827	1.823	1.832
O6–H4–O4′	160.6	162.5	162.9	168.3

3.2. Thermoanalytic investigations

On heating the compounds at least three mass steps are observed in the TG curves that are accompanied with endothermic events in the DTA curves (Fig. 5). It can be assumed that the first step corresponds to the loss of the channel water molecules, whereas in the second step the water molecules coordinated to the metal atoms are emitted. This assumption is supported by the MS measurements that shows that only water ($m/z = 18$) is emitted. Furthermore, elemental analysis of the residues is in good agreement with that calculated for the fully dehydrated compounds (Section 2). The peak temperatures for the second step increase from Mn to Ni, indicating that the bonding interaction between the coordinated water molecules and the metal atoms increases (Fig. 5). For the removal of the channel water molecules no definite trend can be extracted from the

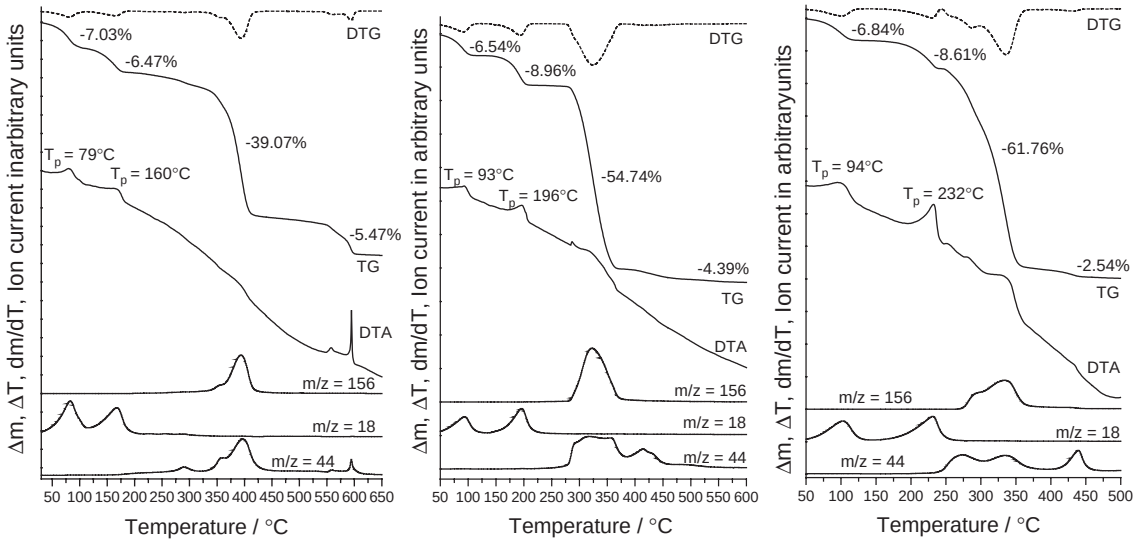

Fig. 5. DTA, TG, DTG and MS trend scan curve for the Fe (left), Co (mid) and Ni (right) compound (heating rate: 4°C/min; $m/z = 18$: water; $m/z = 44$: CO_2 (squarate); $m/z = 156$: 4,4′-bipyridine; given are the mass changes in (%) and the peak temperatures T_p in °C).

decomposition temperatures observed in the DTA curves. The experimental mass loss in both steps are only in rough agreement with that calculated for the removal of three channel water molecules (Δm_{theo}–$3H_2O = 13.05\%$ (Fe), 13.0% (Co) and 13.0% (Ni)) and the two coordinated water molecules (Δm_{theo}–$2H_2O = 8.7\%$ (Fe), 8.7% (Co) and 8.6% (Ni)). We have performed several measurements and we always have found different and mostly smaller values than expected. It is highly likely that a precedent loss of these water molecules occurs during the storage of the samples, which also influences the value of the second mass change.

In the third step the 4,4′-bipyridine ligands are removed ($m/z = 156$) and the squarate dianions decompose ($m/z = 44$). The final products of the reaction were identified as the metal oxides by X-ray powder diffraction.

To investigate the reversibility of the different reaction steps we have performed ex-situ time-dependent X-ray powder measurements for the Ni compound (Fig. 6). Similar measurements were also undertaken for the Fe compound, but the quality of the experimental pattern is very poor due to a strong fluorescence. For the Co compound the partially dehydrated phase is difficult to investigate, because it absorbs immediately water from the atmosphere. If the channel water molecules in the Ni compound were removed in vacuum or by thermal treatment only slightly changes are observed in the powder patterns (Fig. 6). Mainly the intensities of the first two peaks change, indicating that the structures of the hydrated and the partially dehydrated compound are strongly related. Storing this sample in a humid atmosphere for some time the powder pattern of this sample is identical to that of the starting compounds,

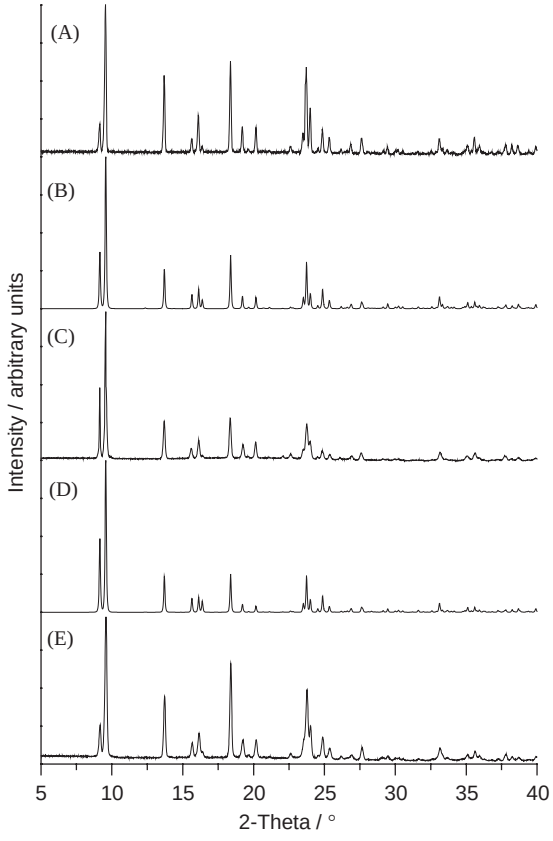

Fig. 6. Ex-situ time-resolved powder patterns for the Ni compound. Powder pattern of a freshly prepared sample (A), after removal of the channel water molecules (C) and after storing this sample in a humid atmosphere (E) as well as calculated powder pattern for the hydrated compound (B) and if the channel water molecules were removed (D) (the pattern of the dehydrated sample was calculated using the single crystal data without consideration of the channel water molecules).

which shows that the process is fully reversible. Similar results were obtained for the Mn compound [28]. From these investigations it can be assumed that the hydration and dehydration process occurs via a topotactic reaction. This assumption is supported by additional investigations using single crystal X-ray experiments. Two complete data sets were measured for a freshly prepared single crystal of the Ni compound and after this crystal was suspended to vacuum for some time. The reflections of the partially hydrated phase can be indexed successfully yielding the same monoclinic metric as for the starting compound with only slight changes in the lattice parameters. The habit of the crystal does not change and only a broadening of some reflections is observed. In addition, we have determined the single crystal structure of all compounds for crystals which were stored in a silica gel filled glassy container so that a part of the channel water molecules was removed in the crystals. All structures could be refined successfully and the positions of the water molecules are only partially occupied and some disordering is present. In addition, the deintercalation of the channel water molecules leads to small but significant changes in the metal coordination and especially of the hydrogen bonds.

To investigate the dehydration process of the water molecules which are coordinated to the metal atoms additional experiments were performed in which freshly prepared samples of the Co and Ni compound were heated in a thermobalance until all water molecules are removed. X-ray powder diffraction of the residues demonstrate that their powder patterns are completely different from those calculated for the starting compounds from single crystal data (Fig. 7). In addition, the reflections are significantly broadened indicating a much smaller crystal size or some strain in the particles. However, if the residues were suspended to a humid atmosphere for some time, the pattern of the starting compounds are retained completely. Therefore, even the removal of the coordinated water molecules is reversible.

To be sure that no additional phases occur during the removal of the water molecules additional experiments with temperature dependent X-ray powder diffraction were conducted (Fig. 8). On heating the Co and Ni compound a continuous change of the reflection positions is observed which is due to an anisotropic change of the lattice parameters. Starting at about 150°C for the Co and at about 110°C for the Ni compound a dramatic alteration of the patterns is observed that can be attributed to the loss of the channel water molecules (Fig. 8). Increasing the temperature leads to a second transformation at about 210°C (Co) and 240°C (Ni) which is due to the removal of the coordinated water molecules. From these investigations there are no hints for the occurrence of additional intermediate phases. The transition temperatures are at higher values than in the DTA-TG measurements because the reaction took place in part in a self-produced atmosphere filled with the water which is emitted by the sample. However, the changes of the powder patterns during these reactions are stronger than those observed in the ex-situ measurements which can be attributed to an anisotropic change of the lattice parameters as function of temperature.

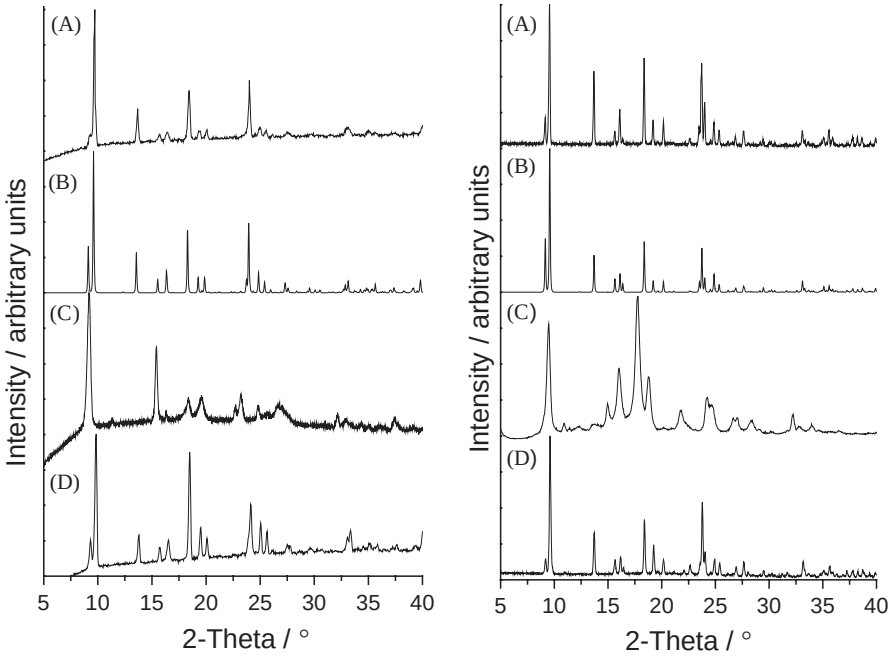

Fig. 7. Ex-situ time-resolved powder patterns for the Co (left) and Ni compound (right). Powder pattern of a freshly prepared sample (A), after complete removal of the water molecules (C) and after storing this sample in a humid atmosphere (D) as well as calculated powder pattern (B).

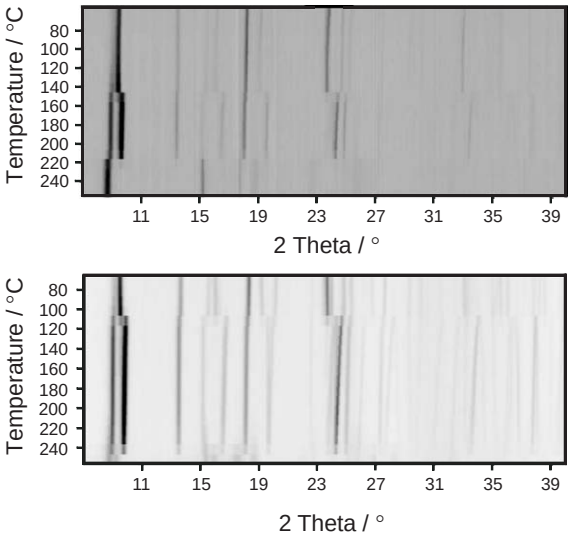

Fig. 8. Temperature-dependent X-ray powder patterns for the Co (top) and Ni compound (bottom) (static air atmosphere; glass capillaries; heating rate: 2°C/min; powder patterns were measured every 5°C).

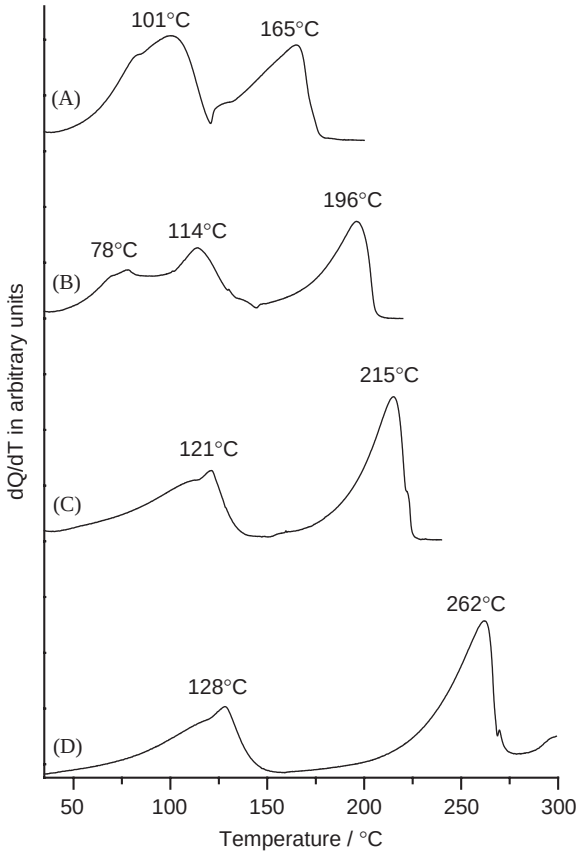

Fig. 9. DSC curves for the Mn (A), Fe (B), Co (C) and Ni (D) compound.

The dehydration reaction was additionally investigated using differential scanning calorimetry (DSC) (Fig. 9). In contrast to the DTA-TG-MS measurements the samples were investigated in pans that contain small holes. Under these conditions the water is only slowly removed and therefore, the atmosphere is saturated with water emitted by the sample. This leads to higher decomposition temperatures and to a better resolution of the thermal events because the hydrated phases are more stable. On heating freshly prepared samples of all compounds, two thermal events are observed in the DSC curves. The first peak corresponds to the removal of the channel water molecules and the second to the emission of the coordinated water molecules (Fig. 9). For the Fe compound two different peaks are observed during the removal of the channel water molecules and the reason for this behavior is not clear. We have performed several measurements and we always observed slightly different curves. However, the increase of the decomposition temperatures from Mn to Ni for the removal of the coordinated water molecules can be attributed to an increase of the bonding interactions. This assumption is supported by an analysis of the thermal energies involved with this step that increase in the same direction. In this context it must be considered that all samples investigated contain slightly different amounts of channel water which also influence the enthalpies estimated from the DSC curves. But it must be stressed that several measurements were done for all compounds which confirm this trend.

As it is obvious from the DSC curves the peak temperatures also increase from Mn to Ni but the onset of the decomposition reactions decreases. For Mn a sharp maximum is found whereas e.g. for Ni a wide peak is observed. For the heavier elements decomposition practically starts at room temperature. This may explain the observation, that we never found single crystals of the Ni compound with fully occupied channels. However, the enthalpies of the first step decrease from Mn to Ni demonstrating that the channel water molecules are removed much easier.

The hydration and dehydration was also investigated with UV-Vis measurements to monitor the change of the color of the materials being associated with the water removal. The colors of the fully hydrated Mn compound is colorless, of Fe orange-red, of Co light pink and of Ni light blue. The colors of the fully dehydrated samples are yellow for Mn, brown for Fe, yellow for Co and yellow for Ni. The spectrum of a fully dehydrated sample of the Ni compound was recorded first and then the sample was stored in a humid atmosphere and was measured again. The spectra were then measured until no change of the spectra could be detected (Fig. 10). As it is obvious a continuous change of the spectra is observed and the intensity of the band at about 650 nm increases with increasing water content. For the Fe and the Co compound only the spectra of the hydrated and fully dehydrated compounds are presented (Fig. 11).

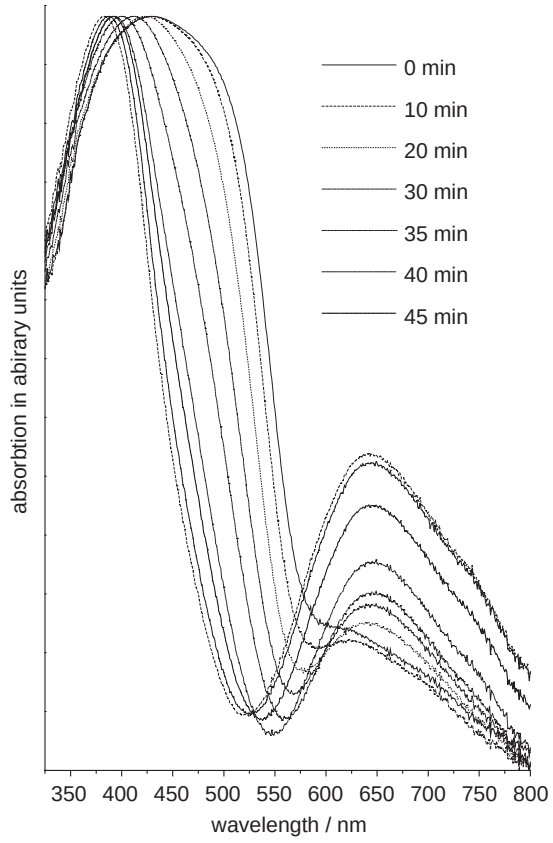

Fig. 10. UV-Vis spectra as function of time if a completely dehydrated sample of the Ni compound is stored in a humid atmosphere.

However, even for this compounds a dramatic change of the spectra is observed.

3.3. Structural changes during the removal of the water molecules coordinated to the metal atoms

Concerning the structural changes during the removal of the coordinated water molecules the X-ray powder patterns of the starting compounds and the partially (only the channel water molecules are removed) dehydrated phases similar but completely different from those of the completely dehydrated (channel + coordinated water molecules are removed) compounds. However, this does not necessarily mean that there is no structural relationship between the hydrated and fully dehydrated phase. We believe that both structures are strongly related due to the interpenetration of the two-dimensional grids. Hence after the removal of the coordinated water molecules, which connect the interpenetrated layers by O–H···O hydrogen bonds the structure should not collapse. But in this case the metal atoms should have only a four-fold coordination environment which is unfavorable. However, the six-fold coordination can be retained by the oxygen atoms of the squarate dianions which are not involved in metal coordination (Fig. 12). Therefore, the hydration and dehydration process of the water molecules that are coordinated to the metal atoms is presumably accompanied by a reversible change of the coordination between the squarate dianions and the metal atoms.

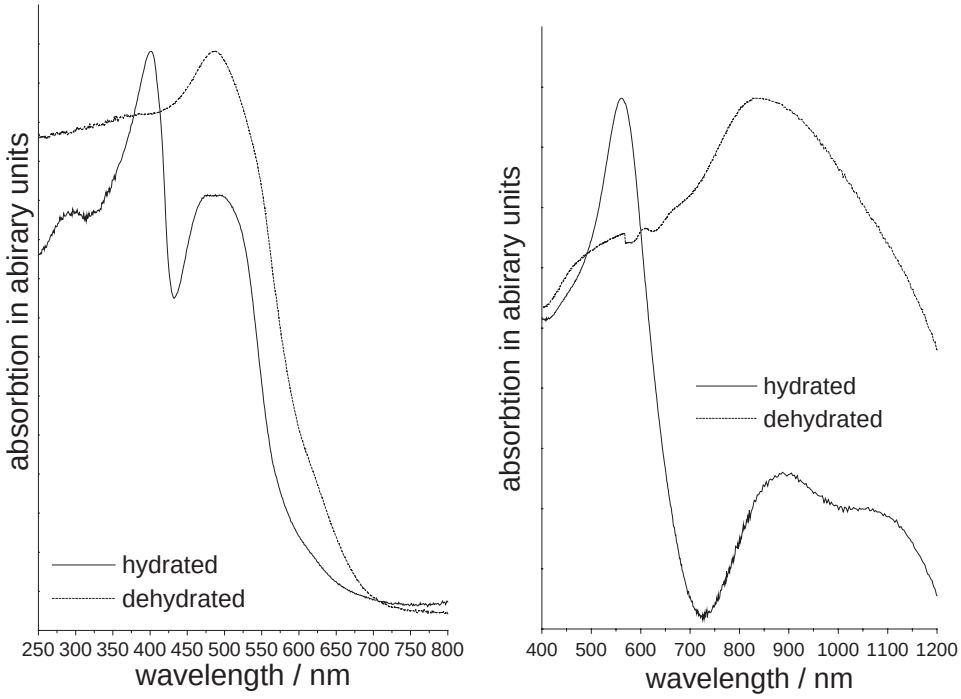

Fig. 11. UV-Vis spectra for the hydrated and fully dehydrated Fe (left) and Co compound (right).

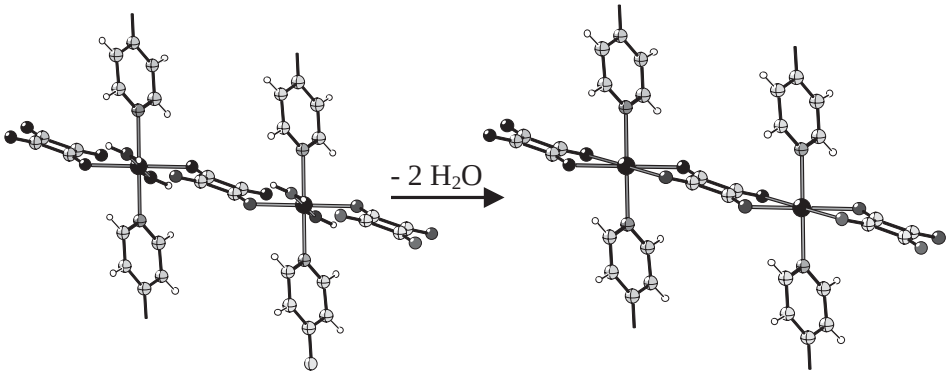

Fig. 12. Part of the crystal structure of the 4,4′-bipyridine metal squarates (*Me* = Mn, Fe, Co, Ni) showing the metal coordination in the hydrated compounds (left) and hypothetical structure of the fully dehydrated compounds (right).

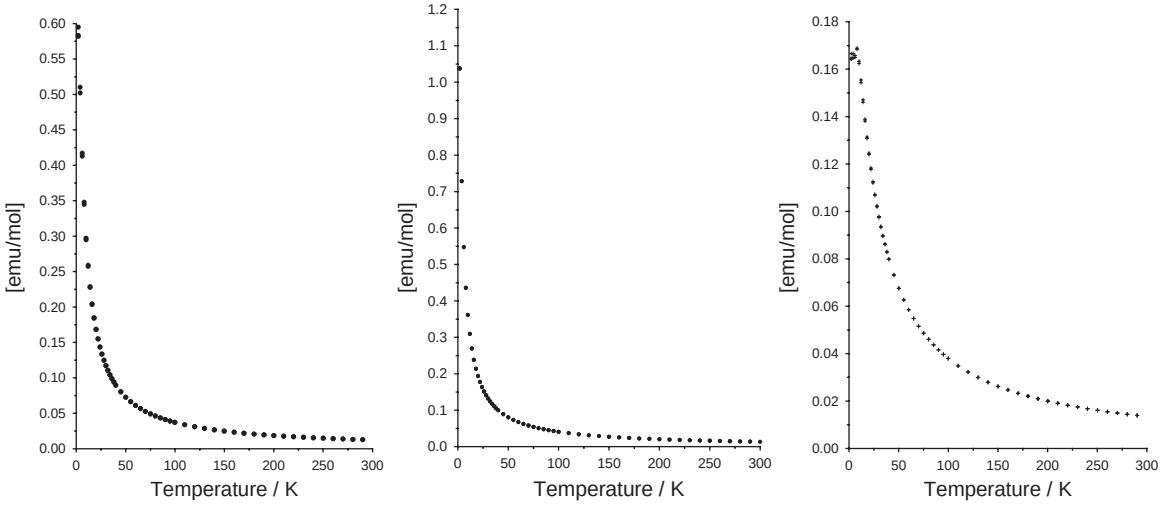

Fig. 13. Results of the magnetic measurements for the hydrated Mn compound (left), the Mn compound in which the channel water molecules are removed (mid) and the fully dehydrated compound (right) (channel water molecules and the water molecules coordinated to the metal atoms are removed).

When the fully dehydrated sample is treated with water these molecules replace one of the two oxygen atoms of the squarate dianion coordinated to the metal atoms. The driving force for this substitution could be the energetically more stable monodentate coordination of the squarate dianion. However, in agreement with this explanation is the observation that in most of the crystal structures of transition metal squarates, the metal atoms are coordinated only by one oxygen atom of the squarate dianions [34–38, 47–49]. Unfortunately we do not know the structure of the fully dehydrated compounds. We have tried several methods to get single crystals and we have tried to solve the structure by powder methods but without any success. However, the proposed mechanism is supported by the results of magnetic measurements on the manganese compound (Fig. 13). The fully and partially hydrated phases shows only a small antiferromagnetic interaction whereas the fully dehydrated phase shows an antiferromagnetic ordering of the spins of the metal atoms at about $T_N = 8$ K. It might be that the exchange in the fully dehydrated sample is mediated by the squarate dianions which should have changed their coordination.

4. Conclusions and outlook

In the present work we have demonstrated that based on simple considerations concerning the nature of the metal atoms and coordination behavior of the ligands the crystal structure of coordination polymers can be controlled to some extent. Whereas the occurrence of two-dimensional grids in these compounds was planned, the formation of the three-dimensional coordination network by interpenetration of these grids was not intended. However, compounds were obtained that contain channels in which additional water molecules are embedded. These channel water molecules can

reversibly be removed in a topotactic reaction. Surprisingly, also the removal of the water molecules which are coordinated to the metal atoms is reversible. The temperature of the steps and the energies involved depend on the nature of the metal atoms and can be understood on the basis of the slightly different crystal structures. The hydration and dehydration processes lead to continuous and significant changes of the optical properties of these compounds which can be attributed to a change of the coordination of the metal atoms. Based on the structural data and the magnetic measurements a mechanism for the removal of the water molecules that are coordinated to the metal atoms is suggested. To prove this assumptions structural and spectroscopic investigations as well as theoretical calculations are planned. However, this will be the subject of further investigations.

Acknowledgments

We gratefully acknowledge the financial support by the State of Schleswig-Holstein. We are very thankful to Professor Dr. Wolfgang Bensch for helpful discussion, financial support and the facility to use his experimental equipment.

References

[1] B. Moulton, M.J. Zaworotko, Chem. Rev. 101 (2001) 1629.
[2] P.J. Hagrman, D. Hagrman, J. Zubieta, Angew. Chem. 111 (1999) 2798; Angew. Chem. Int. Ed. Engl. 38 (1999) 2638.
[3] S.R. Batten, R. Robson, Angew. Chem. 110 (1998) 1558; Angew. Chem. Int. Ed. Engl. 37 (1998) 1460.
[4] R. Robson, Comprehensive Supramolecular Chemistry, Pergamon, New York, 1996, p. 733 (Chapter 22).
[5] R. Robson, B.F. Abrahams, S.R. Batten, R.W. Grable, B.F. Hoskins, J. Liu, Supramolecular Architecture, ACS publications, Washington, DC, 1992 (Chapter 19).
[6] O.M. Yaghi, H. Li, C. Davis, D. Richardson, T.L. Groy, Acc. Chem. Res. 31 (1998) 474.
[7] S.R. Batten, Curr. Opin. Solid State Mater. Sci. 5 (2001) 107.
[8] S.R. Batten, Cryst. Eng. Comm. (2001) 18.
[9] C.B. Aakeröy, A.M. Beatty, Aust. J. Chem. 54 (2001) 409.
[10] A.J. Blake, N.R. Champness, P. Hubberstey, W.-S. Li, M. Schröder, Coord. Chem. Rev. 183 (1999) 17.
[11] B.J. Holiday, C.A. Mirkin, Angew. Chem. 113 (2001) 2076; Angew. Chem. Int. Ed. Engl. 40 (2001) 2022.
[12] B. Moulton, M.J. Zaworotko, Curr. Opin. Solid State Mater. Sci. 6 (2002) 117.
[13] D. Braga, L. Maini, M. Polito, L. Scaccianoce, G. Cijazzi, F. Greponi, Coord. Chem. Rev. 216 (2001) 225.
[14] A. Fu, X. Huang, J. Li, T. Yuen, C. Long Lin, Chem. Eur. J. 8 (2002) 2239.
[15] J.A. Real, G. De Munno, M.C. Munoz, M. Julve, Inorg. Chem. 30 (1991) 2701.
[16] J.S. Haynes, A. Kostikas, J.R. Sams, A. Simopoulos, R.C. Thompson, Inorg. Chem. 26 (1987) 2630.
[17] J. Larionova, R. Clerac, B. Donnadieu, C. Guerin, Chem. Eur. J. 8 (2002) 2712.
[18] Y. Song, S. Ohkoshi, Y. Arimoto, H. Seino, Y. Mizobe, K. Hashimoto, Inorg. Chem. 6 (2003) 1848.
[19] R. Pellaux, H.W. Schmalle, R. Huber, P. Fischer, T. Hauss, B. Ouladdiaf, S. Decurtins, Inorg. Chem. 26 (1997) 2301.
[20] S. Decurtins, H.W. Schmalle, P. Schneuwly, R. Pellaux, J. Ensling, Mol. Cryst. Liq. Cryst. 273 (1995) 167.
[21] R. Sieber, S. Decurtins, H. Stoeckli-Evans, C. Wilson, D. Yufit, J.A.K. Howard, S.C. Capelli, A. Hauser, Chemistry 17 (2001) 361.
[22] H.-L. Sun, B.-Q. Ma, S. Gao, G. Su, Chem. Commun. (2001) 2586.
[23] F. Lloret, M. Julve, J. Cano, G. De Munno, Mol. Cryst. Liq. Cryst. 334 (1999) 569.
[24] J.L. Manson, A.M. Arif, J.S. Miller, Chem. Commun. (1999) 1479.
[25] S. Noro, S. Kitagawa, M. Yamashita, T. Wada, Chem. Commun. (2002) 222.
[26] S.R. Batten, B.F. Hoskins, R. Robson, Chem. Eur. J. 6 (2000) 156.
[27] M.J. Zaworotko, Angew. Chem. 112 (2002) 3180; Angew. Chem. Int. Ed. Engl. 39 (2000) 3052.
[28] T.M. Reineke, M. Eddaoudi, M.O. O'Keeffe, O.M. Yaghi, Angew. Chem. 111 (1999) 2712; Angew. Chem. Int. Ed. Engl. 38 (1999) 2590.
[29] F. Robinson, M.J. Zaworotko, Chem. Commun. (1995) 2413.
[30] O.M. Yaghi, H.L. Li, J. Am. Chem. Soc. 118 (1996) 295.
[31] C. Näther, I. Jeß, Acta Crystallogr. C 57 (2001) 260.
[32] C. Näther, J. Greve, I. Jeß, Z. Naturforsch. 58b (2003) 1.
[33] C. Näther, J. Greve, I. Jeß, Chem. Mater. 14 (2002) 4536.
[34] C.-R. Lee, C.-C. Wang, Y. Wang, Acta Crystallogr. B 52 (1996) 966.
[35] C. Näther, J. Greve, I. Jeß, Acta Crystallogr. E 58 (2002) m507.
[36] C. Näther, J. Greve, I. Jeß, Acta Crystallogr. E 58 (2002) m653.
[37] M. Habenschuss, B.C. Gerstein, J. Chem. Phys. 61 (1974) 852.
[38] A. Ludi, P. Schindler, Angew. Chem. 80 (1968) 664.
[39] G.M. Sheldrick, SHELXS-97, Program for Crystal Structure Solution, University of Göttingen, Germany, 1997.
[40] G.M. Sheldrick, SHELXL-97, Program for the Refinement of Crystal Structures, University of Göttingen, Germany, 1997.
[41] X-Red Program for Data Correction and Data Reduction, Version 1.11, Stoe & Cie, Darmstadt, Germany, 1998.
[42] X-Shape, Program for numerical absorption correction, Version 1.03, Stoe & Cie, Darmstadt, Germany, 1998.
[43] R.D. Shannon, C.T. Prewitt, Acta Crystallogr. B 25 (1969) 925.
[44] R.D. Shannon, Acta Crystallogr. A 32 (1976) 751.
[45] F. Allen, O. Kennard, Chem. Des. Autom. News 8 (1993) 31.
[46] CSD, Conquest, Version 1.2, 1999.
[47] D.S. Yufit, D.J. Price, J.A.K. Howard, S.O.H. Gutschke, A.K. Powell, P.T. Wood, Chem. Commun. (1999) 1561.
[48] A. Weiss, E. Riegler, I. Alt, H. Böhme, C. Robl, Z. Naturforsch. B 41 (1986) 18.
[49] C.-R. Lee, C.-C. Wang, Y. Wang, Acta Crystallogr. B 52 (1996) 966.